THE JOURNAL OF PHYSICAL CHEMISTRY C
Article
Cite This: J. Phys. Chem. C 2018, 122, 5599−5605
pubs.acs.org/JPCC

# Charge Transfer in an Ordered Ag/$Cu_2S$/4-MBA System Based on Surface-Enhanced Raman Scattering

Xin-Yuan Zhang,[†,‡,§,⊥] Donglai Han,[∥,⊥] Zhenyu Pang,[†] Yansen Sun,[†] Yaxin Wang,[§] Yongjun Zhang,[§] Jinghai Yang,[*,§] and Lei Chen[*,§]

[†]Changchun Institute of Optics, Fine Mechanics and Physics, Chinese Academy of Sciences, Changchun 130033, P. R. China
[‡]University of Chinese Academy of Sciences, Beijing 100049, P. R. China
[§]Key Laboratory of Functional Materials Physics and Chemistry of the Ministry of Education, Jilin Normal University, Changchun 130103, P. R. China
[∥]School of Materials Science and Engineering, Changchun University of Science and Technology, Changchun 130022, P. R. China

**ABSTRACT:** In this study, we introduced an ordered metal−semiconductor−molecular system and investigated the surface-enhanced Raman scattering (SERS) effect. The carrier distribution and density can be easily monitored by changing the thickness of the $Cu_2S$ film on the surface of the Ag monolayer under different laser excitations. Meanwhile, different laser wavelengths were selected for investigating the enhancement mechanism of the system based on the viewpoint of the number of carriers and changes in the excitation energy. During this process, we found that the SERS peaks located at 1586 $cm^{-1}$ changed significantly because the intensity can be "borrowed" from exited transition and the molecule-to-semiconductor transition. In combination with the theories of Albrecht and Lombardi, this phenomenon was analyzed in detail, and the experimental results and theoretical research match well. This research regarding the semiconductor-based SERS substrates will expand the basic theory of SERS enhancement and provide a theoretical basis for optical and biological applications.

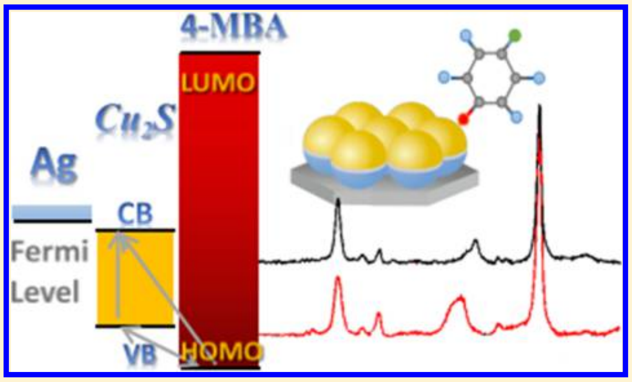

## ■ INTRODUCTION

Raman scattering can provide unique information regarding molecular vibrations; however, the signal intensity is only $10^{-10}$ times that of the incident light. Since its discovery in 1974,[1] surface-enhanced Raman scattering (SERS) exhibited a unique characteristic that perfectly solved the Raman shortcoming.[2,3] As a highly sensitive trace detection technology, SERS has been widely applied in various areas, such as photocatalysis, trace analysis, and semiconductor optoelectronic devices.[4−6] During the past few decades, researchers have been committed to discussing the SERS enhancement mechanism. As we know, there are two major SERS mechanisms: electromagnetic (EM) enhancement mechanism and charge transfer (CT) enhancement mechanism. The EM mechanism exhibits a long-range effect that reflects the interaction between the light and the substrate, and the enhanced signal is a result of the local surface plasmon resonance (LSPR).[7] The LSPR for noble metals always depends on the size, morphology, and dielectric constant of the material. In addition, researchers controlled the position and intensity of the LSPR by tuning various parameters, and many studies have noted that the position can be adjusted in a wide region. The CT mechanism is a short-range effect that shows the chemical interaction between the adsorbed molecule and the metal surface, and light-induced charge transfer is the most important enhancement factor.[8] Nevertheless, a large number of studies have verified that both EM and CT mechanisms independently cannot explain all of the phenomena regarding SERS, and research regarding the enhancement mechanism is still insufficient.

In the 1980s, Yamamoto's group first observed that the Raman signals from pyridine on the surface of semiconductors such as NiO and $TiO_2$ were significantly enhanced, and these results have attracted great interest.[9] During the next few years, many other semiconductors have also been reported to have similar characteristics.[10] However, for the enhancement mechanism of semiconductors, the number and density of free carriers are necessary parameters, which are different from those in metals. To understand the Raman enhancement mechanisms of semiconductor-based substrates, Zhao's group investigated the SERS mechanism from the distribution, density, and motion trends of carriers; moreover, they detailed the pathways of the CT mechanism in semiconductor-based materials.[8,11,12] Additionally, noble metal−semiconductor nanostructures have been synthesized during these years,

**Received:** January 21, 2018
**Revised:** February 17, 2018
**Published:** February 19, 2018

DOI: 10.1021/acs.jpcc.8b00701

Scheme 1. Schematic of the Fabrication Process of the Ag/$Cu_2S$ Ordered Arrays

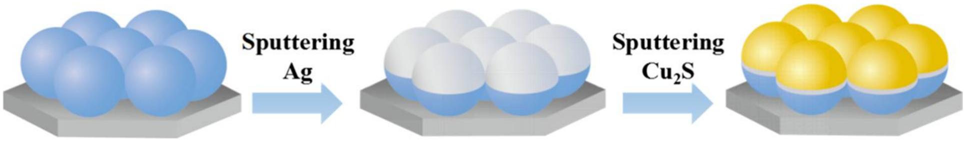

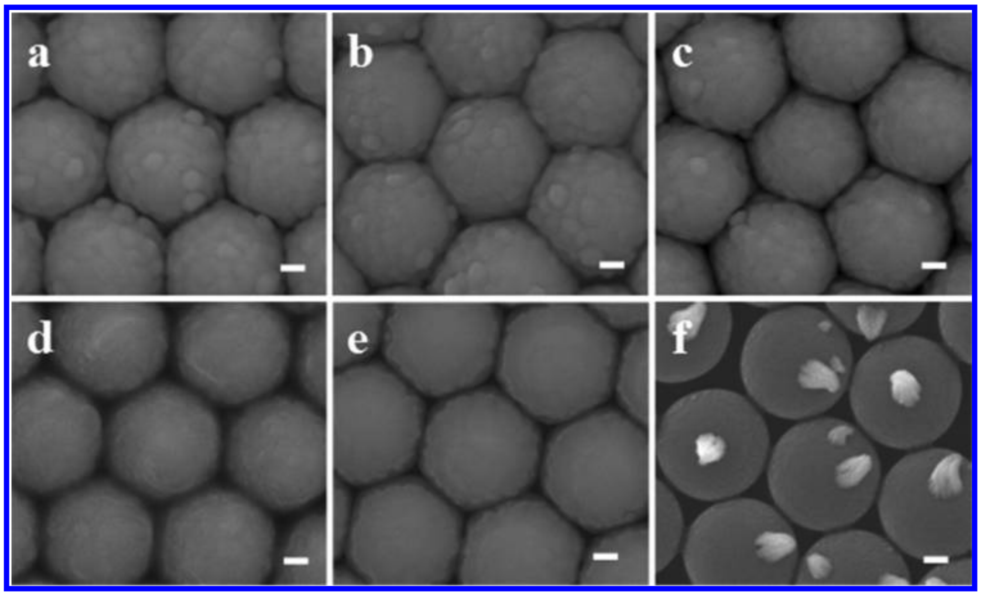

**Figure 1.** SEM images of the composite structure on the PS arrays with various sputtering times: (a) Ag sputter deposition for 10 min at a power of 60 W, (b−e) after Ag sputter deposition for 10 min at a power of 60 W, $Cu_2S$ was sputter deposited for 30, 60, 90, and 120 min at a power of 100 W, and (f) $Cu_2S$ sputter deposition for 30 min. All of the scales above represent 100 nm.

which produced many new properties. Our group fabricated Ag@$Cu_2O$ nanoparticles and changed the frequency of the plasmonic resonance and the distribution and number of carriers by controlling the thickness of the $Cu_2O$ shell, which conspicuously enhanced the Raman signal of 4-mercapobenzonic acid (4-MBA).[13] We presented that this result is due to plasmon-induced SERS. Furthermore, these results provided a new idea for studying the enhancement mechanism of semiconductors. However, most of our studies were limited to wide-band-gap semiconductors, such as ZnO and $TiO_2$, and there are few reports describing the enhancement mechanisms for narrow-band-gap semiconductors.

To extend the semiconductor-based enhancement theory for SERS, the design of a noble metal and a semiconductor with a narrow-band-gap composite material is essential. As we know, noble metals as plasmon materials could achieve the perfect SERS phenomenon, which can contribute to the LSPR effect.[14] However, a plasmon has a specific lifetime, and the main mechanisms for plasmon decay are always via (i) nonradiative transfer, (ii) radiative transfer, (iii) resonance energy transfer, and (iv) uphill electron transfer during direct contract.[4,15] For the uphill electron transfer condition, the plasmon can induce electron−hole pair separation when the metal and semiconductor contract, which is of great importance for photocatalysis, sensing, SERS, and so on.[15,16] In general, the movement of electrons is mainly related to the incident light direction and the contact mode between the metal and semiconductor.

$Cu_2S$, a p-type semiconductor with a narrow band gap (1.2 eV), has been reported as a potential plasma material that could be used for catalytic degradation dyes in the visible-light region.[17] Here, we fabricated an ordered Ag/$Cu_2S$ substrate onto the self-assembled monodispersed polystyrene (PS) particles. We investigated the charge-transfer effect on the SERS of this system, controlled the distribution and density of the carriers by changing the thickness of the semiconductor film, and studied the effect of the carriers on the SERS effect. Meanwhile, the substrates were excited by different laser wavelengths, which provided the charge transfer from the molecules to the semiconductor by the Herzberg−Teller coupling term.[18] These studies will provide a theoretical basis for optical applications.

## ■ EXPERIMENTAL SECTION

**Preparation of the Ordered Metal Arrays.** First, two-dimensional ordered templates were fabricated by using self-assembly technology. To obtain a highly ordered array, a further diluted uniform microsphere particle aqueous solution with a microsphere size of 500 nm (purchased from Bangs Laboratories Inc.) was diffused in ultrapure water (18.25 MΩ $cm^{-1}$) and then sodium dodecyl sulfate (AR, Sigma-Aldrich Co., Ltd.) was added. The arrays were then removed by the prepared silicon wafers (size: 2 × 2 $cm^2$), which were heated in a mixture of $H_2O_2$ (30%, Sinopharm Chemical Reagent Co., Ltd.) and $NH_4OH$ (25%, Sinopharm Chemical Reagent Co., Ltd.), followed by ultrasonic treatment and rotation in ethanol (AR) and ultrapure water. Second, the metal arrays on the microsphere were fabricated by a magnetron sputtering system (ATC 1800-F, USA AJA). Both Ag and $Cu_2S$ targets with a purity of 99.99% were purchased from Beijing TIANRY Science & Technology Development Center. The sputtering time for Ag was 10 min, whereas the sputtering times for $Cu_2S$ were 0, 30, 60, 90, and 120 min. For all of the samples, the sputtering power for Ag was 60 W and that for $Cu_2S$ was 100 W. The base pressure was $2 \times 10^{-5}$ Pa, and the working pressure was 0.6 Pa. Scheme 1 shows the schematic of the fabrication process of the Ag/$Cu_2S$ ordered arrays. For the SERS measurement, 4-mercaptobenzoic acid (4-MBA) (AR, Sigma-Aldrich Co., Ltd.) was used as a probe molecule. The Ag/$Cu_2S$ ordered arrays were immersed in 4-MBA combined with a $10^{-3}$ M ethanol solution for 1 h. Here, all of the chemicals were used without further purification. More detailed methods can be found in our previous work.[19−21]

**Characterization of the Ordered Metal Arrays.** To obtain the morphology of the Ag/$Cu_2S$ arrays, scanning electron microscopy (SEM, JEOL 6500F) and transmission electron microscopy (JEM-2100HR) images were obtained, and both operated at an accelerating voltage of 200 kV. The ultraviolet−visible (UV−vis) absorption spectra were acquired using a Shimadzu UV-3600 spectrometer. The X-ray photoelectron spectra (XPS) were obtained using a Thermo Scientific ESCALAB 250Xi A1440 system, and the XPS spectra were calibrated using carbon (C 1s = 284.6 eV). The analyses were conducted using an Al K$\alpha$ radiation with an energy step size of 1.0 eV. The Raman spectra of the sample were obtained in a Renishaw Raman system model 2000 confocal microscopy spectrometer with a 514 nm excitation source and a Horriba-Jobin-Yvon LabRAM ARAMIS spectrometer with 633 and 785 nm excitation sources.

## ■ RESULTS AND DISCUSSION

As we know, the morphology of the substrate serves as an important parameter that affects the overall performance of the material. The SEM images of the Ag/$Cu_2S$ composite structure on the 500 nm microsphere arrays with various sputtered times are illustrated in Figure 1. In Figure 1a, after the Ag sputter deposition for 10 min, the substrate appeared obviously grainy; however, as the $Cu_2S$ sputtering time increased, the surface appeared to be smooth, as shown in Figure 1b−e. Figure 1f is a SEM image of $Cu_2S$ sputtered for 30 min at a power of 100 W, and the bright cone structure is $Cu_2S$. This structure can be explained by the basic theory of the formation and growth of a film, that is, sputtering deposition needs to go through the processes of nucleation and growth, and this structure is one of the important stages in the growth process.

The different optical properties of the substrates were investigated by UV−vis absorption spectra, as shown in Figure 2. The lines (a)−(f) correspond to the images (a)−(f) in the SEM images. The absorbance of these substrates appears in the visible-light region. For the 500 nm microsphere arrays, there are two peaks at ∼510 and ∼622 nm owing to optical diffraction, as previously reported. Furthermore, the peaks for all of the composite materials here increased to ∼519 nm.[22] In addition, the peaks broadened with the influence of Ag and $Cu_2S$. The absorbance on the blue side of 500 nm is slightly blue-shifted with increasing $Cu_2S$ layer thickness. The band at ∼447 is attributed to the $Cu_2S$ resonance absorbance, and the absorption at ∼449 nm is due to the resonance absorbance of Ag. With increasing $Cu_2S$ content, the peaks are blue-shifted, but with little effect on the peak width.

To further understand the details of the substrates, the XPS spectra were collected and analyzed. The XPS spectra for Ag/$Cu_2S$ with sputtering deposition times for Ag and $Cu_2S$ of 10 and 120 min, respectively, are illustrated in Figure 3 and calibrated by contaminant carbon (C 1s = 284.6 eV). Figure 3a shows the XPS spectral region for Ag 3d. The peaks of Ag $3d_{5/2}$ and Ag $3d_{3/2}$ at 368.6 and 374.6 eV can be assigned to $Ag_2S$ and Ag,[20] which suggests that Ag mainly exists as a simple substance; however, the Ag at the interface constitutes a new chemical bond with sulfur atoms from $Cu_2S$. Figure 3b shows peaks at 933.0 and 952.8 eV, which can be indexed to Cu $2p_{3/2}$ and Cu $2p_{1/2}$ and assigned to $Cu_2S$ and Cu, respectively.[23] Figure 3c presents the XPS spectra of S 2p, and the peaks at 162.2 and 163.4 eV can be assigned to $Cu_2S$ and S, respectively. Additionally, the peaks at 168.6 and 169.9 eV can be ascribed to oxidized sulfur species,[23] but the positions are red-shifted owing to the influence of the inner Ag layer. The peaks in Figure 3d represent the survey spectra and can be assigned to S $2p_{3/2}$, S 2p, C 1s, Ag $3d_{5/2}$, Ag $3d_{3/2}$, O 1s, Cu $2p_{3/2}$, and Cu $2p_{1/2}$, indicating that $Cu_2S$ was deposited on Ag successfully.

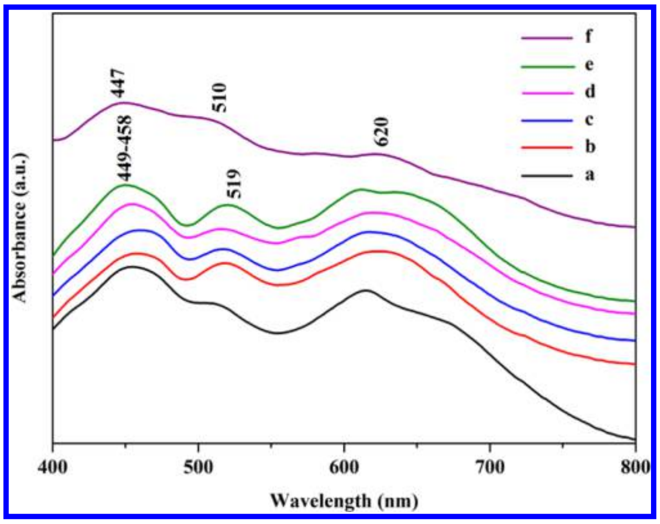

**Figure 2.** UV−vis absorbance spectra for (a) Ag sputter deposition for 10 min, (b−e) after Ag sputter deposition for 10 min, and $Cu_2S$ sputter deposition for 30, 60, 90, and 120 min, and (f) $Cu_2S$ sputter deposition for 30 min. The sputtering power for Ag was 60 W and that for $Cu_2S$ was 100 W.

Figure 4 shows the SERS spectra of the Ag/$Cu_2S$/4-MBA system with various excitation wavelengths. After 4-MBA was adsorbed on Ag/$Cu_2S$, the SERS signals are observed at approximately 997, 1012, 1077, 1138, 1181, 1586, and 1706 $cm^{-1}$, and the assignments of bands are listed in Table 1.[8,13,24] Figure 4a represents the Raman spectra at an excitation wavelength of 514 nm. Figure 4b,c shows the spectra at the excitation wavelengths of 633 and 785 nm, respectively. The peaks at approximately 1425 $cm^{-1}$ in Figure 4a due to $COO^-$ stretching are shifted after $Cu_2S$ sputtering. This finding suggests that 4-MBA might be adsorbed on the surface of $Cu_2S$,[9] and with an increase in the $Cu_2S$ layer thickness, the peak positions are red-shifted, which is more clearly shown in Figure 4b. Meanwhile, at the excitation wavelengths of 633 and 785 nm, the peak shifts also occur at ∼1072 and ∼1573 $cm^{-1}$. These shifts are because the different excitation wavelengths caused different resonance response regions in the substrates and the probe molecules.[12] For this system, all of the peaks have a downward trend, except for the peaks located at ∼1586 $cm^{-1}$, which can be ascribed to $\upsilon$ (CC), an $a_1$ vibration mode. We have chosen the intensities of the peaks located at ∼1586 $cm^{-1}$ to represent the entire spectrum, and the intensity chart for different sputtering times with various excitation wavelengths is shown in Figure 4d. It is obvious that when the

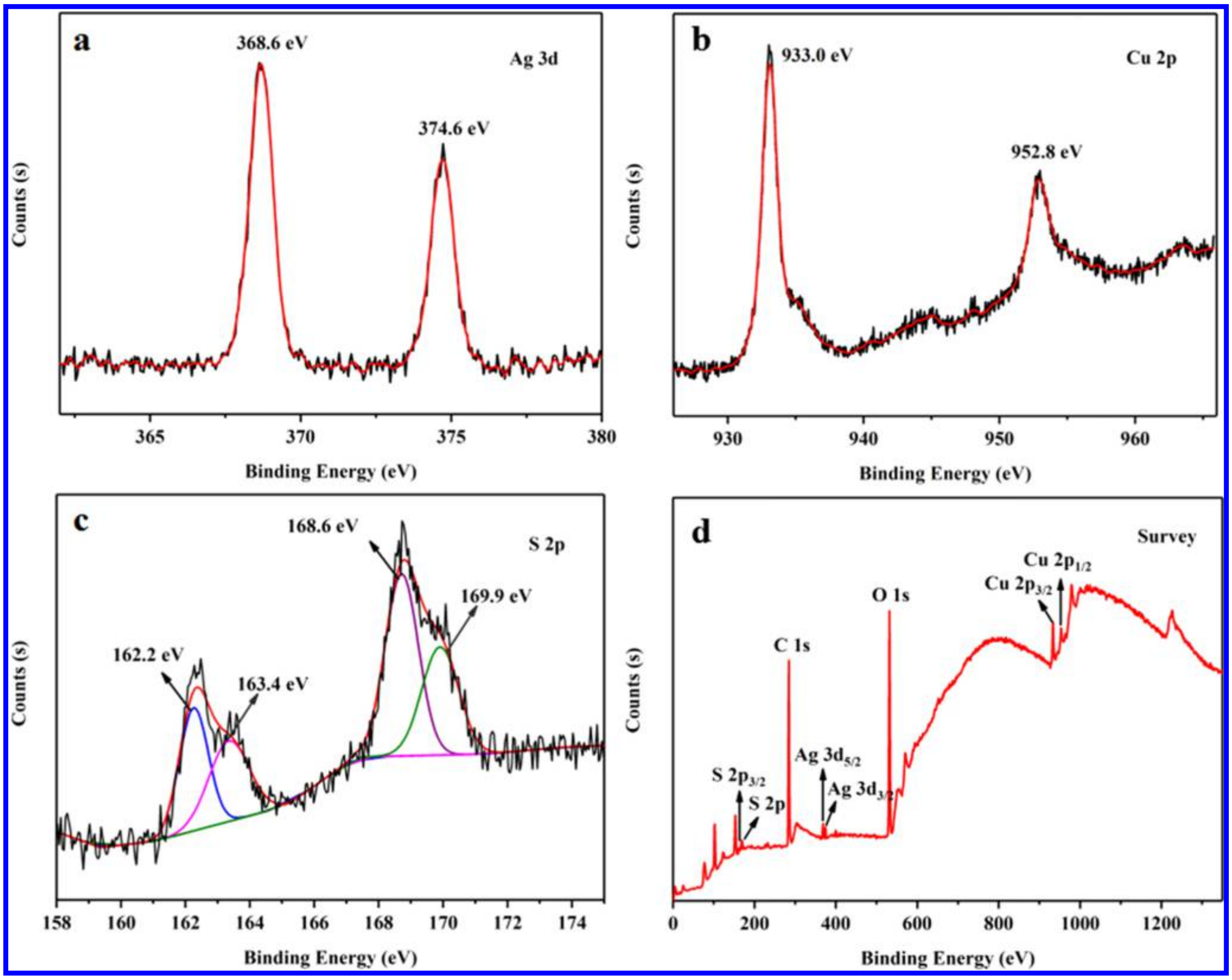

**Figure 3.** XPS spectra for (a) Ag 3d, (b) Cu 2p, and (c) S 2p and (d) the survey spectra of Ag/$Cu_2S$, where the sputtering deposition time for $Cu_2S$ is 120 min.

**Table 1. Wavenumbers and Assignments of the Bands at Various Excitation Wavelengths in the SERS Spectrum of 4-MBA Molecules**[a]

| wavenumbers ($cm^{-1}$) | | | |
|---|---|---|---|
| 514 nm | 633 nm | 785 nm | band assignments |
| 997 | 997 | 990 | in-plane ring breathing, $b_2$ |
| 1012 | 1019 | 1012 | in-plane ring breathing, $b_2$ |
| 1077 | 1072 | 1068 | in-plane ring breathing + $\upsilon$ (C−S), $a_1$ |
| 1138 | 1138 | 1128 | $\upsilon$ (CH), $b_2$ |
| 1181 | 1179 | 1173 | $\upsilon$ (CH), $a_1$ |
| 1586 | 1583 | 1573 | totally symmetric $\upsilon$ (CC), $a_1$ |
| 1706 | 1706 | 1706 | C═O stretching |

[a] $\nu$, stretching; $\gamma$, bending. For ring vibrations, the corresponding vibrational modes of benzene and the symmetry species under $C_{2v}$ symmetry are indicated.

semiconductor is sputtered for 30 min, the signal intensity of the probe molecule was significantly enhanced after the laser irradiation at 514 and 633 nm, which may even be higher than that of Ag. Additionally, with an increase in the sputtering time for $Cu_2S$, the intensity decreases; nevertheless, the signal intensity excited by 785 nm is always decreasing. Of course, that is a noteworthy phenomenon.

To further analyze the detailed information in the spectra and explain this phenomenon, we analyzed the data using the following process.[18,25] Considering the different conditions, the intensity can be expressed as[18]

$$I = [8\pi((\omega \pm \omega_{I'I})^4 I_L / 9c^4] \sum \alpha_{\sigma\rho}^2 \quad (1)$$

where $\omega$ represents the frequency of the incident light, $\omega_{I'I}$ represents a molecular transition between states I and I′, and I and I′ are assumed to be two different vibronic levels of the ground electronic state ($I_e$). The incident light intensity ($I_L$) is a function of the dielectric constant ($\varepsilon$). Here, $\alpha_{\sigma\rho}$ is the polarizability tensor attributed to molecule-to-semiconductor CT transitions, as previously studied by Albrecht ($\sigma$ and $\rho$ are the polarization directions).[26] For the Ag/$Cu_2S$/4-MBA system, the energy level is shown in Figure 5. As reported earlier, this excitation energy from the laser provides an enhanced spectra, the most are observed with excitation close to the charge-transfer transition to "borrow" intensity from the nearby interband transition of $Cu_2S$ at 1.2 eV (5.6−4.4 eV). As we know, the laser energies for the 514, 633, and 785 nm excitations are 2.4, 1.9, and 1.6 eV, respectively, which are high enough to facilitate electron transfer in the semiconductor from the ground state to an excited state. At the same time, once the

DOI: 10.1021/acs.jpcc.8b00701
J. Phys. Chem. C 2018, 122, 5599−5605

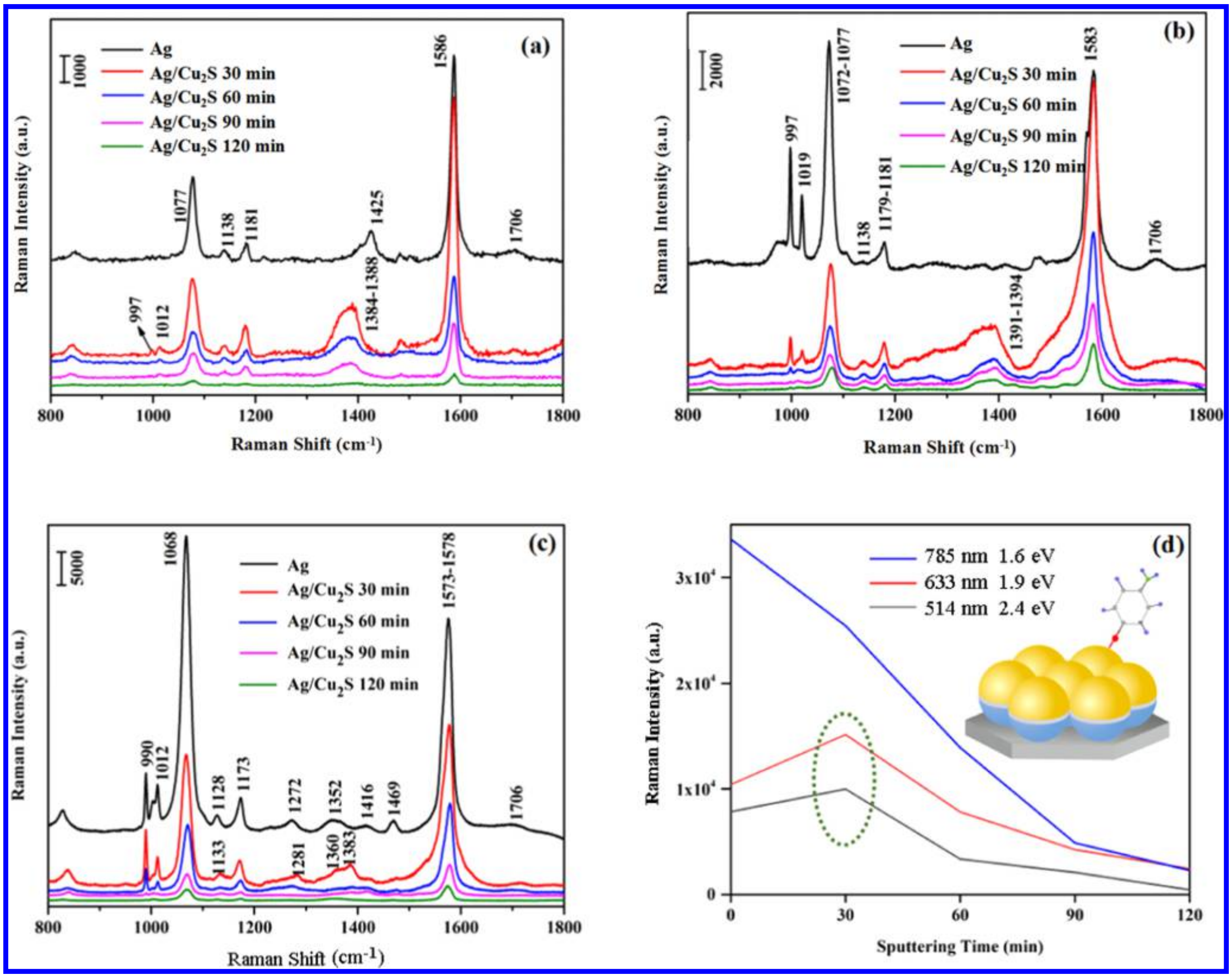

**Figure 4.** SERS spectra of the Ag/Cu$_2$S/4-MBA system with the excitation wavelengths of (a) 514 nm, (b) 633 nm, and (c) 785 nm, and (d) is the peak intensity at 1586 cm$^{-1}$ for different substrates at various excitation wavelengths.

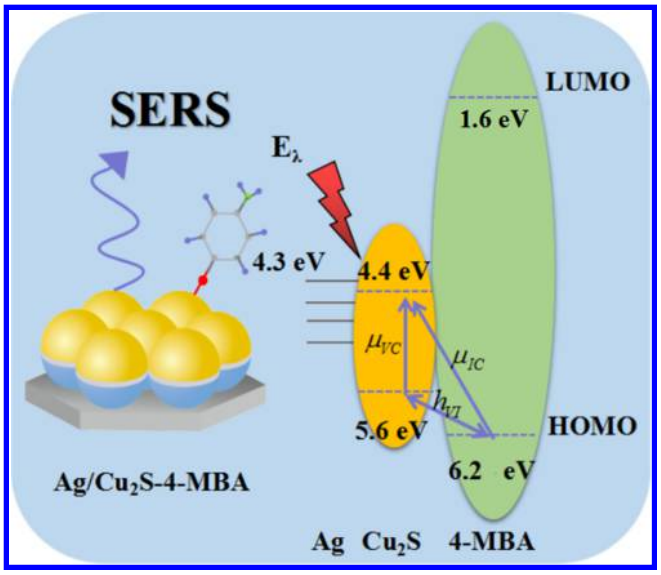

**Figure 5.** Coupling scheme for the Ag/Cu$_2$S/4-MBA system.

energy is sufficiently high, the electrons in 4-MBA will transfer from the highest occupied molecular orbital (HOMO, 6.2 eV) to the conduction band (CB, 4.4 eV) and the valence band (VB, 5.6 eV) in Cu$_2$S. After analyzing the system, the energies for the 514 and 633 nm laser excitations are higher than the band-gap energy between the HOMO and the VB (1.8 eV). Therefore, the intensity also comes from the excited transition and molecule-to-semiconductor transition, which just explained the unusual enhancement for the 514 and 633 nm laser excitations. Therefore, at a laser excitation energy of 785 nm, the intensity mainly contributed to the EM enhancement that comes from Ag; however, in the case of laser excitations at 514 and 633 nm, the intensity is mainly attributed to the synergy between the EM and CT enhancement mechanisms. With the outer semiconductor layer becoming thicker, the EM enhancement will be tremendously restrained, which decreases the peak intensity when the sputtering time of Cu$_2$S is longer than 30 min.

To simplify the system and focus on the resonance, Lombardi's group implied an electric field in the numerator to be paired with the corresponding dipole. The SERS intensity is proportional to $|R|^2$, which can be expressed as[27]

$$R_{\mathrm{ICV}}(\omega) = \frac{\mu_{\mathrm{VC}}\mu_{\mathrm{IC}}h_{\mathrm{VI}}\langle i|Q_k|f\rangle}{((\varepsilon_1(\omega) + 2\varepsilon_0)^2 + \varepsilon_2^2(\omega))((\omega_{\mathrm{IC}}^2 - \omega^2) + \gamma_{\mathrm{IC}}^2)((\omega_{\mathrm{VC}}^2 - \omega^2) + \gamma_{\mathrm{VC}}^2)} \tag{2}$$

where $\gamma$ denotes a damping term, $h_{\mathrm{VI}}$ is the Herzberg−Teller coupling term, $\mu$ is the electric dipole transition moment, and Q is the displacement of the nuclei for a normal mode of the molecule−semiconductor system. The vibrational selection rule maintains a strict harmonic oscillator ($f = i + 1$). Considering the resonance conditions, when the excited energy is stronger (eq 3a) or lower (eq 3b) than the energy between the HOMO and CB, the relations can be expressed as[28]

$$|R_{\mathrm{ICV}}(\omega)|^2 \propto \left| \frac{\mu_{\mathrm{VC}}\mu_{\mathrm{IC}}h_{\mathrm{VI}}}{((\omega_{\mathrm{IC}}^2 - \omega^2) + \gamma_{\mathrm{IC}}^2)((\omega_{\mathrm{VC}}^2 - \omega^2) + \gamma_{\mathrm{VC}}^2)} \right|^2 \tag{3a}$$

$$|R_{\mathrm{ICV}}(\omega)|'^2 \propto \left| \frac{\mu_{\mathrm{VC}}h_{\mathrm{VI}}}{((\omega_{\mathrm{VC}}^2 - \omega^2) + \gamma_{\mathrm{VC}}^2)} \right|^2 \tag{3b}$$

These expressions provide a critical explanation for the phenomenon. Here, $\mu_{\mathrm{VC}}$, $\omega_{\mathrm{VC}}$, and $\gamma_{\mathrm{VC}}$ can be attributed to excited transition, $h_{\mathrm{VI}}$ comes from the Herzberg−Teller coupling, and the left part in eq 3a can be attributed to the molecule-to-semiconductor transition. That is, once the additional energy is lower than the energy between HOMO and CB, the intensity will mainly contribute to the excitation and the nearby interband transition of $Cu_2S$; otherwise, it is important to consider all of the transition conditions. However, the system is influenced significantly by the noble metal Ag, and the thickness of $Cu_2S$ strongly suppressed the strength of the SERS signal.

At present, researchers are devoted to studying the mechanism of SERS and have introduced various parameters into the system. $Cu_2S$, a narrow-band-gap semiconductor material, is an ideal semiconductor-based SERS research agent. After analyzing the SERS spectra, we obtained a critical explanation represented by eq 3a and 3b regarding how the excited light energy and the number of carriers influenced the intensity of the probe molecule on the basis of Albrecht and Lombardi's basic theories in this ordered metal−semiconductor−molecular ($Ag/Cu_2S$/4-MBA) system.

## ■ CONCLUSIONS

In this paper, we designed an $Ag/Cu_2S$/4-MBA system and studied the SERS enhancement. By controlling the carrier distribution and density, the SERS intensities of the probe molecules were clearly influenced. Meanwhile, we excited the substrates with different laser wavelengths and analyzed the SERS spectra on the basis of Albrecht and Lombardi's basic theories, which are well matched with the experimental results. The SERS enhancement model of the $Cu_2S$ film will improve the understanding of the SERS enhancement mechanism in semiconductors, which provides a new method to improve the high sensitivity of the metal/semiconductor composite SERS substrates. This study of semiconductor-based SERS is very important for SERS development and applications.

## ■ AUTHOR INFORMATION

### Corresponding Authors

*E-mail: jhyang1@jlnu.edu.cn (J.Y.).

*E-mail: chenlei@jlnu.edu.cn (L.C.).

### ORCID

Jinghai Yang: 0000-0001-8409-6035

### Author Contributions

$^{\perp}$X.-Y.Z. and D.H. equally contributed to the manuscript.

### Notes

The authors declare no competing financial interest.

## ■ ACKNOWLEDGMENTS

This work was supported by the National Natural Science Foundation of China (Nos. 61775081, 61575080, and 61405072), the Program for the development of Science and Technology of Jilin Province (Nos. 20150519024JH and 20150520015JH), and the Technology of Education Department of Jilin Province (No. 2016-217).

## ■ REFERENCES

(1) Fleischmann, M.; Hendra, P. J.; McQuillan, A. J. Raman Spectra of Pyridine Adsorbed at a Silver Electrode. *Chem. Phys. Lett.* **1974**, *26*, 163−166.

(2) Li, J. F.; Zhang, Y. J.; Ding, S. Y.; Panneerselvam, R.; Tian, Z. Q. Core-Shell Nanoparticle-Enhanced Raman Spectroscopy. *Chem. Rev.* **2017**, *117*, 5002−5069.

(3) Liu, J.; Meng, G.; Li, X.; Huang, Z. Ag-Nanoparticle-Decorated Ge Nanocap Arrays Protruding from Porous Anodic Aluminum Oxide as Sensitive and Reproducible Surface-Enhanced Raman Scattering Substrates. *Langmuir* **2014**, *30*, 13964−13969.

(4) Cialla, D.; Marz, A.; Bohme, R.; Theil, F.; Weber, K.; Schmitt, M.; Popp, J. Surface-Enhanced Raman Spectroscopy (SERS): Progress and Trends. *Anal. Bioanal. Chem.* **2012**, *403*, 27−54.

(5) Stiles, P. L.; Dieringer, J. A.; Shah, N. C.; Van Duyne, R. P. Surface-Enhanced Raman Spectroscopy. *Annu. Rev. Anal. Chem.* **2008**, *1*, 601−626.

(6) Schlücker, S. Surface-Enhanced Raman Spectroscopy: Concepts and Chemical Applications. *Angew. Chem., Int. Ed.* **2014**, *53*, 4756−4795.

(7) Ding, S. Y.; You, E. M.; Tian, Z. Q.; Moskovits, M. Electromagnetic Theories of Surface-Enhanced Raman Spectroscopy. *Chem. Soc. Rev.* **2017**, *46*, 4042−4076.

(8) Wang, Y.; Ji, W.; Sui, H.; Kitahama, Y.; Ruan, W.; Ozaki, Y.; Zhao, B. Exploring the Effect of Intermolecular H-Bonding: A Study on Charge-Transfer Contribution to Surface-Enhanced Raman Scattering Of p-Mercaptobenzoic Acid. *J. Phys. Chem. C* **2014**, *118*, 10191−10197.

(9) Jiang, L.; You, T.; Yin, P.; Shang, Y.; Zhang, D.; Guo, L.; Yang, S. Surface-Enhanced Raman Scattering Spectra of Adsorbates on $Cu_2O$ Nanospheres: Charge-Transfer and Electromagnetic Enhancement. *Nanoscale* **2013**, *5*, 2784−2789.

(10) Gong, M.; Jiang, X.; Du, J.; Li, X.; Han, X.; Yang, L.; Zhao, B. Anatase $TiO_2$ nanoparticles with Controllable Crystallinity as a Substrate for SERS: Improved Charge-Transfer Contribution. *RSC Adv.* **2015**, *5*, 80269−80275.

(11) Zhang, X.; Yu, Z.; Ji, W.; Sui, H.; Cong, Q.; Wang, X.; Zhao, B. Charge-Transfer Effect on Surface-Enhanced Raman Scattering (SERS) in an Ordered Ag NPs/4-Mercaptobenzoic Acid/$TiO_2$ system. *J. Phys. Chem. C* **2015**, *119*, 22439−22444.

(12) Han, X. X.; Ji, W.; Zhao, B.; Ozaki, Y. Semiconductor-Enhanced Raman Scattering: Active Nanomaterials and Applications. *Nanoscale* **2017**, *9*, 4847−4861.

(13) Chen, L.; Sun, H.; Zhao, Y.; Zhang, Y.; Wang, Y.; Liu, Y.; Zhang, X.; Jiang, Y.; Hua, Z.; Yang, J. Plasmonic-Induced SERS Enhancement of Shell-Dependent Ag@$Cu_2O$ Core−Shell Nanoparticles. *RSC Adv.* **2017**, *7*, 16553−16560.

(14) Hsieh, S.; Lin, P. Y.; Chu, L. Y. Improved Performance of Solution-Phase Surface-Enhanced Raman Scattering at Ag/CuO Nanocomposite Surfaces. *J. Phys. Chem. C* **2014**, *118*, 12500−12505.

(15) Tatsuma, T.; Nishi, H.; Ishida, T. Plasmon-Induced Charge Separation: Chemistry and Wide Applications. *Chem. Sci.* **2017**, *8*, 3325−3337.

(16) Liang, S.; Zhou, Y.; Cai, Z.; She, C. Preparation of Porous g-$C_3N_4/Ag/Cu_2O$: A New Composite with Enhanced Visible-Light Photocatalytic Activity. *Appl. Organomet. Chem.* **2016**, *30*, 932−938.

(17) Ding, X.; Zou, Y.; Jiang, J. Au−$Cu_2S$ Heterodimer Formation Via Oxidization of AuCu Alloy Nanoparticles and in Situ Formed Copper Thiolate. *J. Mater. Chem.* **2012**, *22*, 23169−23174.

(18) Lombardi, J. R.; Birke, R. L. A Unified Approach to Surface-Enhanced Raman Spectroscopy. *J. Phys. Chem. C* **2008**, *112*, 5605−5617.

(19) Wang, Y.; Yan, C.; Chen, L.; Zhang, Y.; Yang, J. Controllable Charge Transfer in Ag-$TiO_2$ Composite Structure for SERS Application. *Nanomaterials* **2017**, *7*, No. 159.

(20) Chen, L.; Sun, H.; Zhao, Y.; Gao, R.; Wang, Y.; Liu, Y.; Zhang, Y.; Hua, Z.; Yang, J. Iron Layer-Dependent Surface-Enhanced Raman Scattering of Hierarchical Nanocap Arrays. *Appl. Surf. Sci.* **2017**, *423*, 1124−1133.

(21) Wang, Y.; Zhao, X.; Gao, W.; Chen, L.; Chen, S.; Wei, M.; Gao, M.; Wang, C.; Zhang, Y.; Yang, J. Au/Ag Bimetal Nanogap Arrays with Tunable Morphologies for Surface-Enhanced Raman Scattering. *RSC Adv.* **2015**, *5*, 7454−7460.

(22) Wang, J.; Zhou, F.; Duan, G.; Li, Y.; Liu, G.; Su, F.; Cai, W. A Controlled Ag−Au Bimetallic Nanoshelled Microsphere Array and Its Improved Surface-Enhanced Raman Scattering Effect. *RSC Adv.* **2014**, *4*, 8758−8763.

(23) Zhang, L.; Zhao, Y.; Zhong, L.; Wang, Y.; Chai, S.; Yang, T.; Han, X. $Cu_2S$-Cu-$TiO_2$ Mesoporous Carbon Composites for the Degradation of High Concentration of Methyl Orange under Visible Light. *Appl. Surf. Sci.* **2017**, *422*, 1093−1101.

(24) Wang, X.; Zhou, L.; Lai, W.; Jiang, T.; Zhou, J. Bifunctional 4MBA Mediated Recyclable SERS-Based Immunoassay Induced by Photocatalytic Activity of $TiO_2$ Nanotube Arrays. *Phys. Chem. Chem. Phys.* **2016**, *18*, 23795−23802.

(25) Lombardi, J. R.; Birke, R. L. Theory of Surface-Enhanced Raman Scattering in Semiconductors. *J. Phys. Chem. C* **2014**, *118*, 11120−11130.

(26) Lombardi, J. R.; Birke, R. L. The Theory of Surface-Enhanced Raman Scattering. *J. Chem. Phys.* **2012**, *136*, No. 144704.

(27) Alessandri, I.; Lombardi, J. R. Enhanced Raman Scattering with Dielectrics. *Chem. Rev.* **2016**, *116*, 14921−14981.

(28) Ji, W.; Kitahama, Y.; Xue, X.; Zhao, B.; Ozaki, Y. Generation of Pronounced Resonance Profile of Charge-Transfer Contributions to Surface-Enhanced Raman Scattering. *J. Phys. Chem. C* **2012**, *116*, 2515−2520.